Demonstration of high speed optical transmission at 2 μm in titanium dioxide waveguides

Manon Lamy, Christophe Finot, Julien Fatome, Juan Arocas, Jean Claude Weeber, Kamal Hammani

Demonstration of high speed optical transmission at 2 µm in titanium dioxide waveguides

MANON LAMY, CHRISTOPHE FINOT, JULIEN FATOME, JUAN AROCAS, JEAN-CLAUDE WEEBER AND KAMAL HAMMANI*

Laboratoire Interdisciplinaire Carnot de Bourgogne (ICB), UMR 6303 CNRS – Université de Bourgogne Franche-Comté, 9 Avenue Alain Savary, BP 47870, 21078 Dijon Cedex, FRANCE
** kamal.hammani@u-bourgogne.fr*

Abstract: We demonstrate the optical transmission of a 10-Gbit/s data signal in the 2 µm waveband into titanium dioxide waveguides. Error-free transmissions have been experimentally achieved taking advantage of a fiber-to-fiber grating-based injection solution.

OCIS codes: (130.0130) Integrated optics; (130.3130) Integrated optics materials; (050.2770) Gratings; (060.4510) Optical communications;

References and links

1. D. J. Richardson, "Filling the Light Pipe," Science 330, 327-328 (2010).
2. N. Kavanagh, M. Sadiq, K. Shortiss, H. Zhang, K. Thomas, A. Gocalinska, Y. Zhao, E. Pelucchi, P. O. Brien, F. H. Peters, B. Corbett, and F. C. G. Gunning, "Exploring a new transmission window for telecommunications in the 2 µm waveband," in 18th International Conference on Transparent Optical Networks (ICTON 2016), 2016), 1-4.
3. Z. Li, A. M. Heidt, J. M. O. Daniel, Y. Jung, S. U. Alam, and D. J. Richardson, "Thulium-doped fiber amplifier for optical communications at 2 µm," Opt. Express 21, 9289-9297 (2013).
4. N. Ye, M. R. Gleeson, M. U. Sadiq, B. Roycroft, C. Robert, H. Yang, H. Zhang, P. E. Morrissey, N. Mac Suibhne, K. Thomas, A. Gocalinska, E. Pelucchi, R. Phelan, B. Kelly, J. O'Carroll, F. H. Peters, F. C. Garcia Gunning, and B. Corbett, "InP-Based Active and Passive Components for Communication Systems at 2 µm," J. Lightwave Technol. 33, 971-975 (2015).
5. M. U. Sadiq, M. R. Gleeson, N. Ye, J. O'Callaghan, P. Morrissey, H. Y. Zhang, K. Thomas, A. Gocalinska, E. Pelucchi, F. C. G. Gunning, B. Roycroft, F. H. Peters, and B. Corbett, "10 Gb/s InP-based Mach-Zehnder modulator for operation at 2 µm wavelengths," Opt. Express 23, 10905-10913 (2015).
6. H. Zhang, M. Gleeson, N. Ye, N. Pavarelli, X. Ouyang, J. Zhao, N. Kavanagh, C. Robert, H. Yang, P. E. Morrissey, K. Thomas, A. Gocalinska, Y. Chen, T. Bradley, J. P. Wooler, J. R. Hayes, E. Numkam Fokoua, Z. Li, S. U. Alam, F. Poletti, M. N. Petrovich, D. J. Richardson, B. Kelly, J. O'Carroll, R. Phelan, E. Pelucchi, P. O'Brien, F. Peters, B. Corbett, and F. Gunning, "Dense WDM transmission at 2 µm enabled by an arrayed waveguide grating," Opt. Lett. 40, 3308-3311 (2015).
7. M. N. Petrovich, F. Poletti, J. P. Wooler, A. M. Heidt, N. K. Baddela, Z. Li, D. R. Gray, R. Slavík, F. Parmigiani, N. V. Wheeler, J. R. Hayes, E. Numkam, L. Grűner-Nielsen, B. Pálsdóttir, R. Phelan, B. Kelly, J. O'Carroll, M. Becker, N. MacSuibhne, J. Zhao, F. C. G. Gunning, A. D. Ellis, P. Petropoulos, S. U. Alam, and D. J. Richardson, "Demonstration of amplified data transmission at 2 µm in a low-loss wide bandwidth hollow core photonic bandgap fiber," Opt. Express 21, 28559-28569 (2013).
8. H. Zhang, N. Kavanagh, Z. Li, J. Zhao, N. Ye, Y. Chen, N. V. Wheeler, J. P. Wooler, J. R. Hayes, S. R. Sandoghchi, F. Poletti, M. N. Petrovich, S. U. Alam, R. Phelan, J. O'Carroll, B. Kelly, L. Grüner-Nielsen, D. J. Richardson, B. Corbett, and F. C. Garcia Gunning, "100 Gbit/s WDM transmission at 2 µm: transmission studies in both low-loss hollow core photonic bandgap fiber and solid core fiber," Opt. Express 23, 4946-4951 (2015).
9. P. J. Roberts, F. Couny, H. Sabert, B. J. Mangan, D. P. Williams, L. Farr, M. W. Mason, A. Tomlinson, T. A. Birks, J. C. Knight, and P. S. J. Russell, "Ultimate low loss of hollow-core photonic crystal fibres," Opt. Express 13, 236-244 (2005).
10. K. Xu, L. Sun, Y. Xie, Q. Song, J. Du, and Z. He, "Transmission of IM/DD Signals at 2 µm Wavelength Using PAM and CAP," IEEE Photonics J. 8, 1-7 (2016).
11. J. Kischkat, S. Peters, B. Gruska, M. Semtsiv, M. Chashnikova, M. Klinkmüller, O. Fedosenko, S. Machulik, A. Aleksandrova, G. Monastyrskyi, Y. Flores, and W. Ted Masselink, "Mid-infrared optical properties of thin films of aluminum oxide, titanium dioxide, silicon dioxide, aluminum nitride, and silicon nitride," Appl. Opt. 51, 6789-6798 (2012).

12. K. Shang, S. S. Djordjevic, J. Li, L. Liao, J. Basak, H.-F. Liu, and S. J. B. Yoo, "CMOS-compatible Titanium Dioxide Deposition for Athermalization of Silicon Photonic Waveguides," in CLEO: 2013, OSA Technical Digest (online) (Optical Society of America, 2013), CF2I.5.
13. J. D. B. Bradley, C. C. Evans, J. T. Choy, O. Reshef, P. B. Deotare, F. Parsy, K. C. Phillips, M. Lončar, and E. Mazur, "Submicrometer-wide amorphous and polycrystalline anatase TiO2 waveguides for microphotonic devices," Opt. Express 20, 23821-23831 (2012).
14. O. Reshef, K. Shtyrkova, M. G. Moebius, S. Griesse-Nascimento, S. Spector, C. C. Evans, E. Ippen, and E. Mazur, "Polycrystalline anatase titanium dioxide microring resonators with negative thermo-optic coefficient," J. Opt. Soc. Am. B 32, 2288-2293 (2015).
15. J. T. Choy, J. D. B. Bradley, P. B. Deotare, I. B. Burgess, C. C. Evans, E. Mazur, and M. Lončar, "Integrated TiO2 resonators for visible photonics," Opt Lett 37, 539-541 (2012).
16. M. Häyrinen, M. Roussey, A. Säynätjoki, M. Kuittinen, and S. Honkanen, "Titanium dioxide slot waveguides for visible wavelengths," Appl Optics 54, 2653-2657 (2015).
17. C. C. Evans, C. Liu, and J. Suntivich, "Low-loss titanium dioxide waveguides and resonators using a dielectric lift-off fabrication process," Opt. Express 23, 11160-11169 (2015).
18. C. C. Evans, K. Shtyrkova, J. D. B. Bradley, O. Reshef, E. Ippen, and E. Mazur, "Spectral broadening in anatase titanium dioxide waveguides at telecommunication and near-visible wavelengths," Opt. Express 21, 18582-18591 (2013).
19. M. Lamy, K. Hammani, J. Arocas, C. Finot, and J. Weeber, "Broadband metal grating couplers embedded in Titanium dioxide waveguides " submitted, preprint available at https://hal.archives-ouvertes.fr/hal-01503970.
20. S. Scheerlinck, J. Schrauwen, F. Van Laere, D. Taillaert, D. Van Thourhout, and R. Baets, "Efficient, broadband and compact metal grating couplers for silicon-on-insulator waveguides," Opt. Express 15, 9625-9630 (2007).

1. Introduction

Nowadays, the communication traffic continuously increases approaching inexorably a 'capacity crunch' [1] : the conventional C-band around 1.55 µm will not be sufficient anymore and alternative approaches have to be adopted. Recently, the 2 µm spectral region has been suggested as a new transmission window [2] benefiting from the emergence of thulium doped fiber amplifier (TDFA) with broadband and high gain spanning from 1900 nm to 2100 nm [3]. This has stimulated studies of dedicated photonic components such as InP-based modulators [4, 5] or arrayed waveguide grating [6]. High bit rate communications over distances exceeding a hundred meters have already been successfully demonstrated [7, 8] in low-loss hollow core bandgap photonic fibers designed to present minimal losses around 2000 nm [9] or in solid-core single mode fibers [10].

Optical transmissions over much shorter distances (a few hundreds of micrometers) also deserve interest in the context of on-board connections and photonic routing and therefore require experimental investigations to evaluate the potentially of various material transparent in this new spectral band. If silicon nitride (Si_3N_4) has already stimulated many works, titanium dioxide (TiO_2) remains to date relatively unexplored. This cost-efficient material is however transparent from the visible to the mid-infrared wavelengths [11] and can be considered as a complementary metal-oxide semiconductor (CMOS) compatible material [12] with an easier deposition process possible at lower temperatures. Compared to Si_3N_4, it presents lower stress constraints for thickness beyond 250 nm and it exhibits a higher linear refractive index which is critical for a stronger confinement [13]. Up to now, detailed studies have taken advantage of its negative thermo-optic coefficient [12, 14] and of its transparency in the visible [15, 16] or have studied its linear and nonlinear properties in the C-band [13, 17, 18]. In this paper, we experimentally explore, for the first time, TiO_2 as a material for photonic component operating at 2 µm. After having described the design and fabrication of TiO_2 waveguides, we detail the experimental setup under use and the validation of the device for error-free transmission of a 10 Gbit/s on-off keying signal.

2. Design and fabrication of the photonic structure

2.1 Design of the input and output grating couplers

Whatever the platform involved for the design, a critical issue in integrated photonics is always to efficiently couple the light into the device. In a dedicated article [19], we have

recently investigated and experimentally validated a new kind of metal gratings that are embedded directly within the dielectric layer instead of being deposited on it [20]. Thus we have been able to couple efficiently a 1.55 µm signal into a TiO_2 photonic waveguide. Here, similar design is used as pictured in Fig. 1(a). More precisely, the structure consists of a metal (Au) grating embedded between two TiO_2 layers on a glass substrate.

Using a commercial finite element based software, we can optimize the parameters of the design to obtain the best coupling around the 2 µm wavelengths. We have taken into account the fabrication and experimental setup constraints, leading to a fixed value of the bottom layer height h_{bottom}=70 nm and of the incident angle Θ = 30°. Thus, using a Monte Carlo algorithm, the coupling efficiency could reach 52 % for TM mode when h_{Au} = 57 nm, h_{top} = 234 nm, Λ = 1904 nm and w_1= 980 *nm*. However, with these parameters, the coupling efficiency for the TE mode drops down to 10 %. Similarly, the optimization of parameters for TE mode gives an efficiency reaching up to 36 % for h_{Au} = 45 nm, h_{top} = 234 nm, Λ = 1679 nm and w_1 = *356 nm* whereas those parameters give a poor efficiency of 1 % for TM mode.

However, contrary to [17], our aim is not to reach the best coupling efficiency. Here we tried to find numerically the geometric parameters that allow a fair coupling efficiency in both TE and TM modes for a slab. From the previous optimization, the top layer should be 234 nm and given that h_{bottom} = 70 nm, the total TiO_2 thickness considered is 304 nm. The thickness of the gold lines h_{Au} is chosen to be 56 nm while the period Λ = 1900 nm. To adjust the efficiency of the TM mode compared to the TE mode, we adjust the filling factor related to the width w_1 as shown in Fig. 1(b). It appears that three values of w_1 allow a similar coupling for TE and TM modes but the width of the grating lines that gives the best efficiency (-8.5 dB) is around 700 nm.

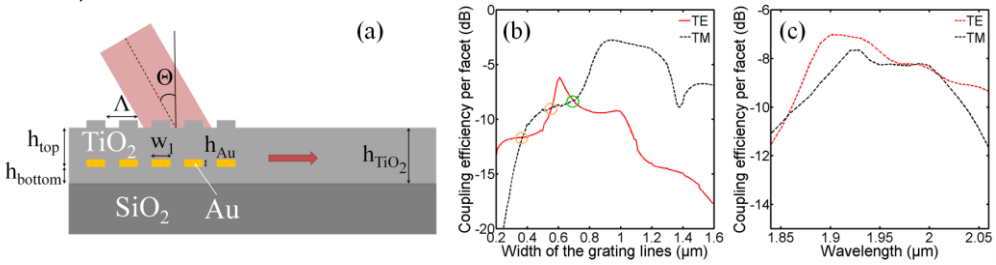

Fig. 1. (a) Embedded metal gratings in TiO_2 layout. (b) Numerical simulations of the coupling efficiency for one facet as a function of the width w_1 of the grating lines for the following parameters: h_{bottom} = 70 nm h_{Au} = 56 nm, h_{top} = 234 nm, Λ = 1900 nm at the central wavelength of our laser source (1.98 µm). The results for TE mode are compared to TM mode. The circles highlight the values where the efficiencies of both modes are equals. The green circle corresponds to the best value. (c) Corresponding coupling efficiency per facet for TE and TM mode as a function of the wavelength (for w_1 = 700 nm - green circle on panel (b)).

2.2 Modal analysis

Here, we focus our attention on two waveguides: a 8.0 µm wide waveguide and a subwavelength 1.6 µm-wide waveguide.

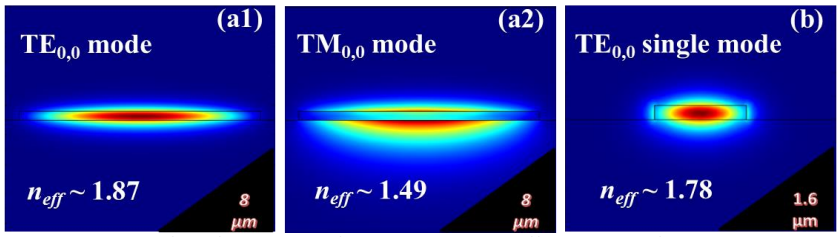

Fig. 2. Mode profile of the electric field and associated effective index for (a) a multimode waveguide (width 8 µm) and (b) a subwavelength waveguide (width 1.6 µm). Subplot (a1) corresponds to the fundamental TE mode whereas subplot (a2) is related to fundamental TM mode.

The 8 µm wide waveguide is clearly multimode with nine TE modes and three TM modes. Figure 2 (a) shows the first TE and TM modes in the multimode (MM) waveguide having an effective index of 1.87 and 1.49 respectively. The subwavelength 1.6 µm wide waveguide is single-mode (SM) with an effective index of the TE mode around 1.78.

2.3 Fabrication

The fabrication process relies on traditional techniques. The titanium dioxide layers are deposited on a glass substrate by reactive DC magnetron sputtering of a 99.9 % pure titanium target under argon and oxygen control atmosphere. A first electron-beam lithography, followed by thermal gold evaporation (here 3 nm of chromium are used as an adhesion layer) and a lift-off process, is used to fabricate the gold gratings. Then the top layer of TiO_2 is deposited followed by an overlay electron-beam lithography. After a metallic mask evaporation, a reactive ion etching is performed to make the waveguides. Finally, a wet etching removes the mask to get the final device to test.

As mentioned previously, we have fabricated two structures of interest (Fig. 3): a MM waveguide (8 µm width) and a SM waveguide (slightly overexposed leading to a width of 1.65 µm). These waveguides have the same length fixed at 575 µm but, for the SM waveguide, two tapers are used at the input and output. The parameters measured on the fabricated device differ slightly from the targeted one: we have measured a 304 nm total thicknesss with h_{bottom} = 69 nm and h_{top} = 235 nm. Moreover, the waveguide width is actually 1.65 µm which induces the existence of the $TE_{0,1}$ with an effective index close to 1.47.

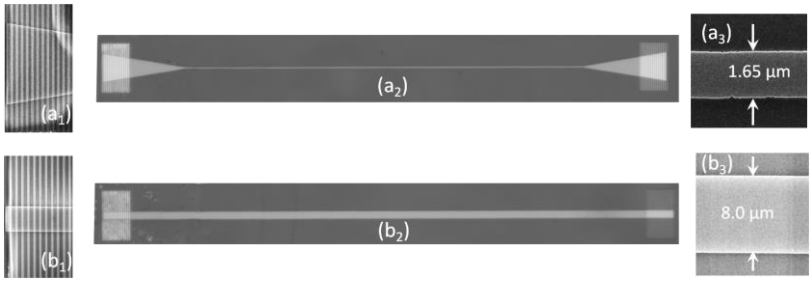

Fig. 3. Images of (a) a subwavelength waveguide and (b) a large waveguide considered as a slab. Insets 1 show SEM pictures of embedded metal grating on one end of waveguides whereas insets 2 show optical images of waveguides. Contrary to the slab, the subwavelength waveguide is equipped with tapers. Insets 3 corresponds to SEM pictures of the subwavelength that has a width of 1.65 µm (a3) and the slab which is actually 8.0 µm wide (b3).

2.4 Test of the device

We have then characterized the coupling efficiency of the waveguides with a setup similar to Ref. [19]. Two focusers oriented with an angle of 30° are used to inject and collect the signal at the input and output gratings respectively. The injection of light emitted by an amplified spontaneous emission (ASE) source spanning from 1900 nm to 2050 nm is adjusted thanks to two cameras operating in the visible and 2 µm ranges. After transmission in the waveguide and decoupling by the grating, the output light is collected by a lensed-fiber focuser and recorded with an optical spectrum analyzer (OSA). Figure 4 presents the total losses as a function of the injected wavelength for the two waveguides under test. Note that those transmission spectra are normalized with respect to a reference spectrum obtained by optimizing the light collected by the output focuser after specular reflection of the incident light onto a gold mirror [19]. We can notice, in Fig. 4, oscillations of high amplitude and short period that are particularly marked for the large waveguide. These spectral oscillations are attributed to a Fabry-Perot effect, the spectral range between two maxima being in agreement with what can be expected from the roundtrip distance. The discrepancy between the numerical simulations and the maximum experimental efficiency is about 3 dB mainly

because of the strong dependency on the width of the grating lines and probably also fabrication issues (related to the roughness). Even though, for the MM waveguide configuration, the TE mode was expected to be as efficient as the TM mode for a grating line width of 700 nm, here it was the case for w_1 = 630 nm. Regarding the TE SM waveguide, as expected, the coupling efficiency is similar to the one obtained for the large waveguide. Let us once again recall that a (6 dB) better efficiency can be reached for optimized parameters but our goal was here to establish a fair comparison between the MM and SM components.

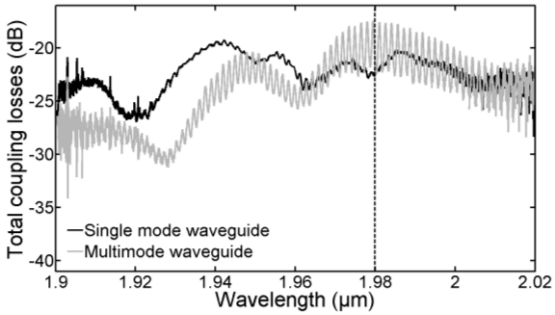

Fig. 4. Total losses as a function of the injected wavelength for a MM waveguide (grey curve) and a SM waveguide (black curve) obtained with the ASE source. The oscillations of short period on the grey curve are due to a Perot-Fabry effect. The grey dashed line corresponds to the central wavelength of the laser source used in the next section.

3. Validation of the transmission of a 10 Gbit/s signal

In order to demonstrate the suitability of our TiO_2 devices for 2 µm telecommunications, we have implemented the experimental setup detailed in Fig. 5. The transmitter (TX) is based on a laser diode centered at 1980 nm that is then intensity modulated by a commercial Niobate-Lithium modulator. The Non-Return-to-Zero On-Off-Keying signal under test is a 2^{31}-1 pseudorandom bit sequence (PRBS) at 10 Gbit/s. Since the photonic waveguides are polarization-sensitive, a polarization controller is used after the intensity modulator. Then a first thulium doped fiber amplifier (TDFA) is used before a 90/10 coupler allowing us to monitor the power injected into the waveguide. Note that the variable optical attenuator is usually implemented just in front of the receiver but due to limited sensitivity of the available powermeters working at 2 µm, it was more convenient to put it before the waveguide.

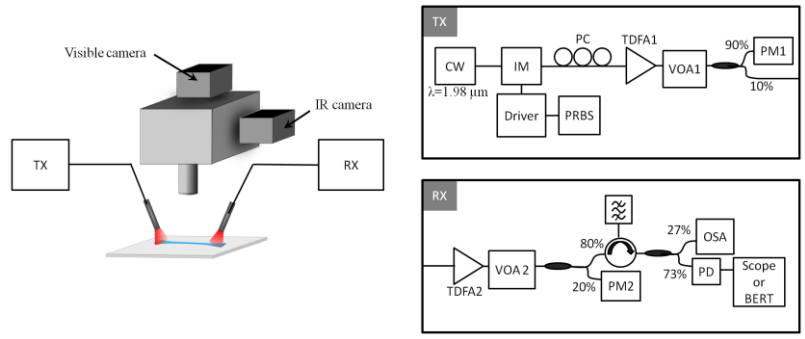

Fig. 5. Experimental setup for a 10 Gbit/s optical transmission. CW : continuous wave ; IM : intensity modulator ; PC : polarization controller ; PRBS : pseudorandom binary sequence ; TDFA : thulium doped fiber amplifier ; VOA : variable optical attenuator ; PM : powermeter ; OSA : optical spectrum analyzer ; PD : photodiode ; BERT : bit error rate tester.

The receiver (RX) is based on a second TDFA. This TDFA works with a constant gain and not with a constant output power as usually used in C-band. Therefore a variable optical attenuator is positioned at its output to ensure that the photodiode operates at a constant power. An optical bandpass filter (0.2 nm bandwidth) is also inserted in order to limit the

accumulation of amplified spontaneous emission from the TDFAs. The signal is finally analyzed in the spectral and temporal domains. An optical spectrum analyzer is used to measure the optical signal-to-noise ratio (OSNR) of the received signal whereas a photodiode (12.5 GHz electrical bandwidth) enables bit error rates measurements as well as recording of the output eye diagram on a high-speed sampling oscilloscope.

Fig. 6 summarizes the results obtained at 1980 nm. Error-free operation can be achieved for back-to-back measurements as well as in the presence of the TiO_2 waveguides. Examples of the corresponding eye-diagrams are provided in panels (a): in both configurations, a widely open eye can be recorded and the insertion of the waveguides under test does not induce any visible degradations of the transmission.

The quality of the transmission through the TiO_2 waveguide is more quantitatively evaluated by the measurement of the Bit Error Rate (BER) according to the OSNR on the photodiode. Results obtained for the various configurations are summarized on Fig. 6(b): the observed trends are very similar, with a very moderate penalty in the presence of the waveguides. No significant difference can be made between the SM and MM waveguides. Therefore, for the length of propagation under consideration, the multimode character of the waveguide does not seem to impair the transmission quality.

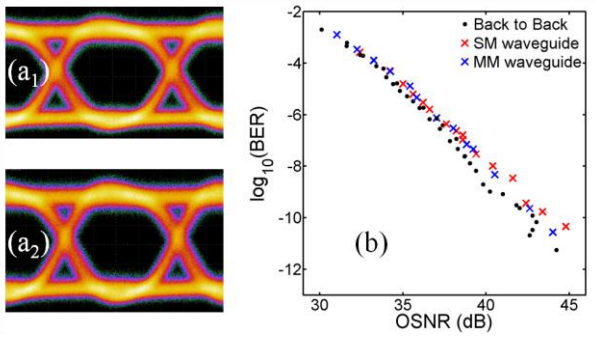

Fig. 6. (a) Eye diagrams for the back to back configuration and after transmission in the 1.5 µm wide waveguide transmission (panels 1 and 2 respectively). In both cases, eyes diagrams have been recorded for error-free measurements. (b) BER as function of OSNR for the two previously described waveguides. On the graph, the black points of measurements are associated with back-to-back configuration. The crosses are used for BER measurements for TiO_2 devices (red for the1.65 µm SM waveguide and blue for the 8 µm wide MM waveguide).

4. Conclusion

To conclude, thanks to embedded metal gratings, we have been able to efficiently couple an incident light beam into a TiO_2 waveguide in the 2 µm spectral range. This particular design allows us to demonstrate, for the first time, an error-free transmission of a 2-µm optical data stream at 10 Gbit/s in a 575-µm long TiO_2 waveguide. A full set of BER measurements has been performed with a fair comparison between a SM 1.65 µm wide waveguide and a multimode 8 µm wide waveguide insensitive to the polarization. No significant difference was then observed.

This study paves the way to integrated photonics at 2 µm and introduces the titanium dioxide as a serious candidate for photonics from the visible to the mid-infrared. With the technological progress and the maturity gain that can be expected in the near future for fiber and optoelectronics solutions operating around 2 µm, we are confident in the possibility to involve longer TiO_2 waveguides up to a few centimeter length.

Acknowledgments

This work is financially supported by PARI PHOTCOM Région Bourgogne, by the Agence Nationale de la Recherche (Labex Action ANR-11-LABX-0001-01), by Carnot Arts Institute (PICASSO 2.0 project). and by FEDER-FSE Bourgogne 2014/2020.